

Application of synthesizing tri-metallic Zn and Ag co-doped TiO₂ nano-photocatalyst by a one-step synthesis technique in treating water pollutants

M. Ghorbanpour^{a,*}, A. Feizi^b

^aTechnical and Engineering Faculty, Department of Chemical Engineering, University of Mohaghegh Ardabili, Ardabil, Iran, email: ghorbanpour@uma.ac.ir (M. Ghorbanpour)

^bTechnical and Engineering Faculty, Department of Civil Engineering, University of Mohaghegh Ardabili, Ardabil, Iran

Received 7 December 2019; Accepted 8 May 2020

ABSTRACT

The present trend in synthesis techniques in the wastewater treatment is altering from the more achievement of a product with the desired properties to methods that are highly effective, economical, and environmentally friendly. In the present work, Zn and Ag co-doped TiO₂ tri-metallic nanoparticles are synthesized by the molten salt method, which is applied as an effective nano photocatalyst for the removal of methyl orange from the aqueous media. The effect of dopant content on the de-colorization of the methyl orange solution has been optimized by the response surface methodology. The prepared nanomaterial was characterized by the X-ray diffraction, diffusive reflectance spectroscopy, and scanning electron microscopy (SEM). In the pure and single metal doping TiO₂ nanoparticles, only the anatase phase was formed. The silver, anatase, and rutile phase could be observed. The pure titanium sample has a band gap of 3.2 eV. All samples have a band gap below this value. The accumulated spherical shaped particles with relatively the same size are available the pure samples. The SEM images show the co-doping results in the formation of larger particles. The experimental results showed that the prepared nanoparticles have a high photo-degradation tendency to remove methyl orange from the aqueous solution under visible light irradiation. The highest photocatalytic activity of 94.2%, belongs to samples containing 0.38% silver and 0.13% zinc.

Keywords: Wastewater treatment; Tri-metallic nanoparticles; Photodegradation; Molten salt synthesis

1. Introduction

Over the past few decades, TiO₂ has been considered as the most promising photocatalyst because of its application in the treatment of pollutants in water and air, which is due to its high photocatalytic activity, excellent functionality, high chemical stability, thermal stability and non-toxicity [1]. However, the effective photo-excitation of TiO₂ requires the radiation of light with an energy level higher than the TiO₂ band gap energy. Consequently, TiO₂

requires UV light with a wavelength of less than 387 nm to be excited and capable of photo-oxidation [2,3]. This practically rules out the use of sunlight as an energy source for the photoreaction on pure TiO₂. Besides, TiO₂ contains a high rate of recombination tendency between the excited electron and the positive hole [3]. Therefore, there is an urgent need to develop a new photocatalyst capable of working under the sunlight/visible light irradiation. In fact, in an ideal situation, the visible photocatalyst should work in open environments and under solar light irradiation, where there is

* Corresponding author.

not any filter. The effectiveness of TiO₂ as a photocatalyst depends on its crystal phase, particle size, and crystallinity, which are greatly influenced by the preparation methods [4]. Therefore, many investigations have been focused on improving the photocatalytic activity of TiO₂ using various dopants [3–8]. In this approach, doping and co-doping of metal ions into TiO₂ (bimetallic and tri-metallic nanoparticles) is one of the effective methods to control the surface properties by harvesting the visible region of the solar spectrum [9–11]. The previous works showed that the tri-metallic nanoparticles have higher catalytic selectivity and activity than their monometallic nanoparticles due to the synergistic effects of their components [10].

Today, different techniques have been used to prepare TiO₂ nanoparticles [12]. Although all of these reports showed excellent results, there are complicated multistep processes in which precision control is important [13]. Here, a very simple, fast, inexpensive, one-step, and the solvent-free process is reported using a newly developed molten salt synthesis to manufacture pure tri-metallic nanoparticles [5–7]. Normal molten salt synthesis is a method in which salt or mixture of salt(s) in the molten state is used as a highly reactive medium. In this method, the intimate mixing of the particles and enhanced (liquid state) diffusion occurs, which accelerates the formation of the product structure. It is faster than the solid-state reaction, and the phase and crystallite habit of certain orientation (depending on relative surface energies) can be obtained at a lower temperature. Eutectic salt compositions are usually employed to achieve maximum reactivity at a minimum temperature [14]. The main difference between the molten salt method presented in this study and the conventional methods is the absence of salt mixtures such as sodium chloride, sodium phosphate, etc. [15]. Thus, the present trend is simpler and produces nanoparticles with higher purity and crystallinity than the normal molten salt methods [1,16].

In this paper, a straightforward approach is proposed using the molten salt method for obtaining tri-metallic Zn and Ag co-doped TiO₂ nanoparticles. The effect of dopant content on the de-colorization of the methyl orange solution has been optimized by the response surface methodology (RSM). The morphology and microstructure of the prepared nanoparticles have been studied by the X-ray diffraction (XRD), diffusive reflectance spectroscopy (DRS), and scanning electron microscopy (SEM).

2. Experimental

All chemicals, including methyl orange, TiO₂, AgNO₃, and ZnCl₂ were purchased from Merck Co., (Germany) and applied without further purification.

2.1. Synthesis nanoparticles

Appropriate amounts of AgNO₃, ZnCl₂, and TiO₂ (Table 1) were completely mixed, milled, and blended to distribute the three compounds evenly in the final mixture. The resulting mixture is then ordered in a furnace at 700°C for 60 min. Then, the prepared nanoparticles were washed adequately with distilled water. After dissolution, the nanoparticles were dried in an oven at 25°C.

Table 1
Factors and their levels

Variable	Real values of coded levels			
	-α	-1	1	+α
Ag	0.375	0	1.5	1.125
Zn	0.125	0	0.5	0.375

2.2. Experimental design and optimization by RSM

The purpose of using the surface response design is to determine the optimum doping content of Zn and Ag in co-doped TiO₂ nanoparticles to obtain the maximum degradation efficiency of dye with the minimum number of experiments. The central composite experimental design, which is widely used for response surface method (RSM), was applied. Two experimental factors at two levels were taken into consideration as follows: Ag (g/g) and Zn (g/g). The operating ranges and levels of the investigated independent variables in this study are given in Table 1. It should be noted that in all samples, the weight of applied titanium dioxide powder was constant and equal to 1 g. The amounts of silver nitrate and zinc chloride salts used during the synthesis step are calculated so that they correspond to the amount provided in the table. The 2-factor design matrix and experimental results obtained in the photocatalytic degradation and mineralization runs are presented in Table 2. To find out the interaction between the selected variables and their response, an analysis of variance (ANOVA) was carried out.

2.3. Characterization

The morphology of samples was observed with a SEM (LEO 1430VP, Germany). UV-vis diffuse reflectance spectroscopy (DR UV-Vis) was taken in the wavelength range of 200–800 nm using a spectrophotometer (Scinco S4100, South Korea). The powder XRD analysis was done using a PW 1050 diffractometer (Philips, The Netherlands) with a Ni filter and Cu Kα (λ = 1.54 Å) radiation.

2.4. Photocatalytic activity

The photocatalytic activity of the nanoparticles was measured by the photodegradation of MO with the initial concentration and volume of 30 ppm and 50 mL, respectively. First, the mixed MO and photocatalyst solution was stirred in the dark for 10 min to equilibrate the absorption/desorption between dye molecules and photocatalyst. Then, it was irradiated at room temperature by a 90 W halogen lamp (Philips, Netherlands). After the reaction, the solution was immediately centrifuged, and its absorbance was measured to calculate the percentage of degradation using the UV-visible spectrophotometer. The photocatalytic degradation efficiency is calculated according to the following equation:

$$\text{Degradation efficiency (\%)} = \left(\frac{A_0 - A}{A_0} \right) \quad (1)$$

where A_0 represents the initial absorption of the dye solution and A denotes the initial absorption after irradiation.

3. Results and discussion

3.1. Characterization

The XRD patterns of pure and doped TiO_2 powders are shown in Fig. 1. A noticeable diffraction peak appeared at $2\theta = 25.3^\circ$, which is observed on the un-doped sample spectrum, is associated with the (101) orientation plane of the anatase crystalline phase of TiO_2 [16].

Like pure nanoparticles, samples 6 and 12 only contain the anatase peaks. The similarity of these two samples is

Table 2
2-factor central composite design matrix along with the observed responses

Standard	Run	Ag	Zn	Photocatalytic activity
0	0	0	0	
3	1	1.13	0.38	93.4
12	2	0.75	0.25	93.3
13	3	1.50	0.25	57.7
6	4	0.75	0.25	92.1
5	5	0.38	0.13	94.2
11	6	0	0.25	59.3
1	7	0.38	0.38	91.6
4	8	0.75	0.25	91.6
9	9	1.13	0.13	73.4
2	10	0.75	0.25	90.2
10	11	0.75	0.50	92.8
8	12	0.75	0	55.4
7	13	0.75	0.25	93.1

that they only contain doped silver or zinc. Therefore, single metal doping preserves the crystallite structure of the primary nanoparticles. This is in agreement with the results of studies on doping with iron, copper, and silver prepared in a similar way to this study [5–7]. In all of these studies, the only formed phase was the anatase phase. In some samples, the XRD peak located at around 27.4° is related to the rutile phase [10]. Furthermore, after doping, the anatase phase peak was preserved in all samples except samples 3 and 9. In these two samples, only the rutile phase is present. Samples 1 and 2 also show a very weak anatase peak with the rutile phase. The similarity of all these four samples is the high amount of silver present in their structure that results in the rapid phase transformation of TiO_2 to the rutile phase. According to the present reports, rutile TiO_2 has two notable advantages over anatase TiO_2 . First, the rutile TiO_2 has a smaller band gap than anatase. Second, the rutile TiO_2 is the most stable TiO_2 phase even in strongly acidic or basic environments [17].

On the other hand, the peaks appeared at around 27.0° , 32.2° , 38.1° , 44.3° , and 46.2° corresponded to the formation of the silver phase according to the 04–0783 standard card from JCPDS [18]. The silver peak is observed in all samples except for samples 6 and 12 and pure nanoparticles. The silver peak is observed in all samples except for samples 6 and 12 and pure nanoparticles. The similarity of sample 6 and 12 are in silver or zinc doping alone. Therefore, single metal doping does not form a phase corresponding to the doped metal. This is consistent with the results of previous studies [6,7].

Using the Scherrer equation, the crystallite size of pure titanium nanoparticles was calculated as 53 nm. This value is somewhat lower in doped samples. For example, crystallite sizes of samples 1, 2, 5, and 7 are equivalent to 43, 41, 50, and 49 nm. Therefore, the co-doping has reduced the size of nanoparticles. The results are consistent with previous research on silver and zinc-doped titanium dioxide

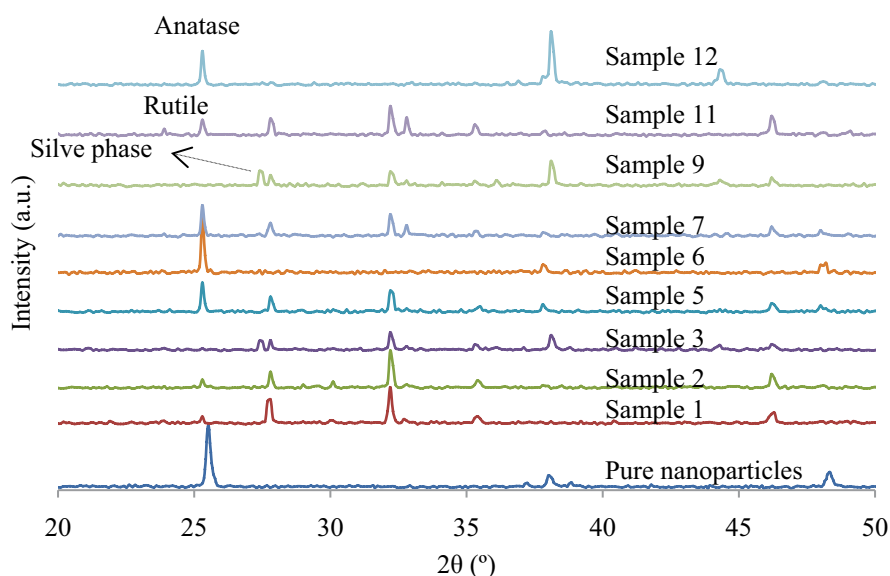


Fig. 1. XRD patterns of pure and co-doped TiO_2 powders.

nanoparticles using the method applied in the present study [6–8].

Fig. 2 shows the optical absorption spectra of pure TiO_2 and co-doped TiO_2 nanoparticles. The spectra of all of the synthesized samples are approximately similar to that of pure TiO_2 . The only major difference (samples 1, 3, and 9) is that the new peak is observed at around 390 nm. This is due to the high silver content of these composites, and consequently, the surface plasmon resonance associated with it. The band gap of the prepared nanoparticles can be calculated by $(Ah\nu)^2$ vs. $h\nu$ plot (Fig. 2b. in this plot, A , h , and ν are the absorbance, the Planck constant and the frequency of incident light, respectively). The band gap of the prepared nanoparticles is calculated by $(Ah\nu)^2$ vs. $h\nu$ plot (Fig. 2b). In this plot, A , h , and ν denote the absorbance, the Planck constant and the frequency of incident light, respectively. This plot indicates a graph with a linear region the extrapolation of which to x -axis provides the band gap value.

The calculated band gap for each sample is summarized in Table 3. The pure titanium sample has a band gap of 3.2. According to Table 3, all samples have a band gap below this value. Samples 12 and 6 have been doped only with silver and zinc, respectively. The band gaps for these samples are 3.14 and 3.0 eV, respectively. Therefore, the presence of both

metals together seems to have a synergistic effect on the band gap so that the samples containing both metals have a lower band gap. Besides, as mentioned in the previous section, the presence of the rutile phase reduces the band gap.

In the case of visible-light-induced photocatalyst with an acceptable activity, the band gap must be less than 3 eV. By referring to Table 3, samples 1, 2, 3, and 9 have the band gap less than 3 eV. As mentioned earlier, in these samples, the amount of silver in the structure is more massive. Therefore, the results indicate a successful reduction of the band gap of the TiO_2 nanoparticles. This indicates the usability of these photocatalysts under the sunlight.

The SEM images of pure and co-doped TiO_2 powders are shown in Fig. 3. The accumulated spherical shaped particles with relatively the same size are seen in pure samples (Fig. 3a). As can be seen, this state is almost preserved in some samples (samples 1, 2, 5, and 6). Like the pure nanoparticles, these samples contain nanoparticles with relatively uniform size. However, some particles may be more massive. This difference is highlighted in other examples. In these examples, larger particles with diverse shapes are easily recognizable. Among these, samples 3 and 9 are quite large, but in samples 7, 11, and 12, along with the larger particles, some nanoparticles are stabilized on the surface of

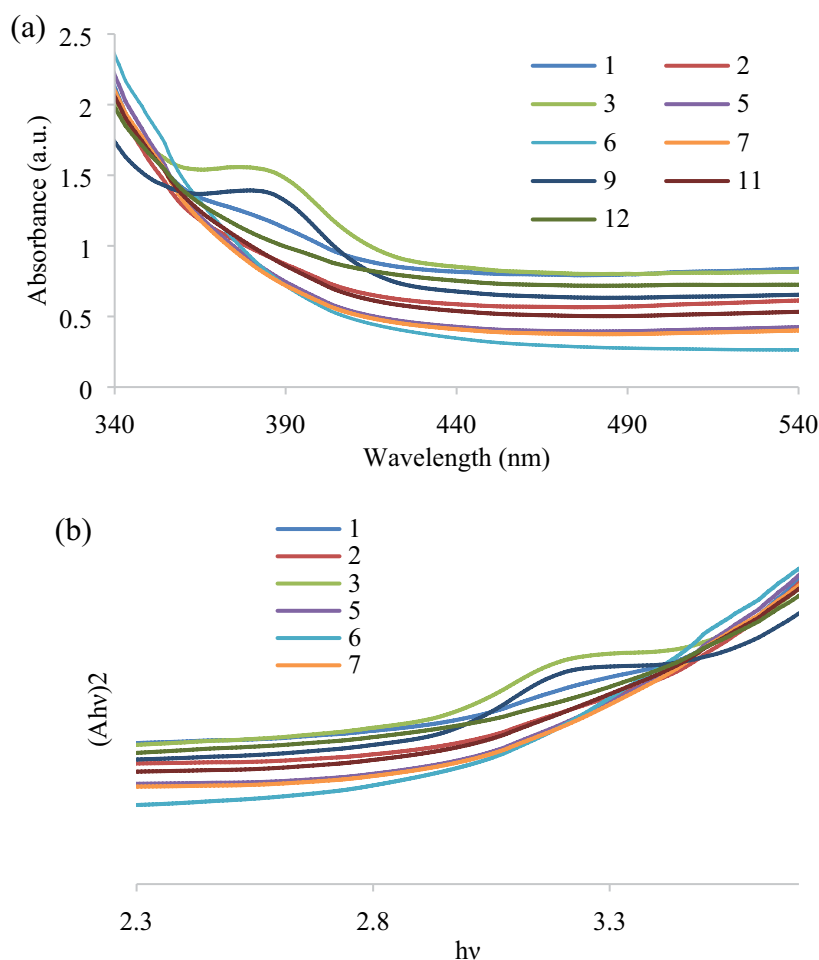


Fig. 2. UV/vis spectra (a) and band gap (b) of pure and co-doped TiO_2 powders.

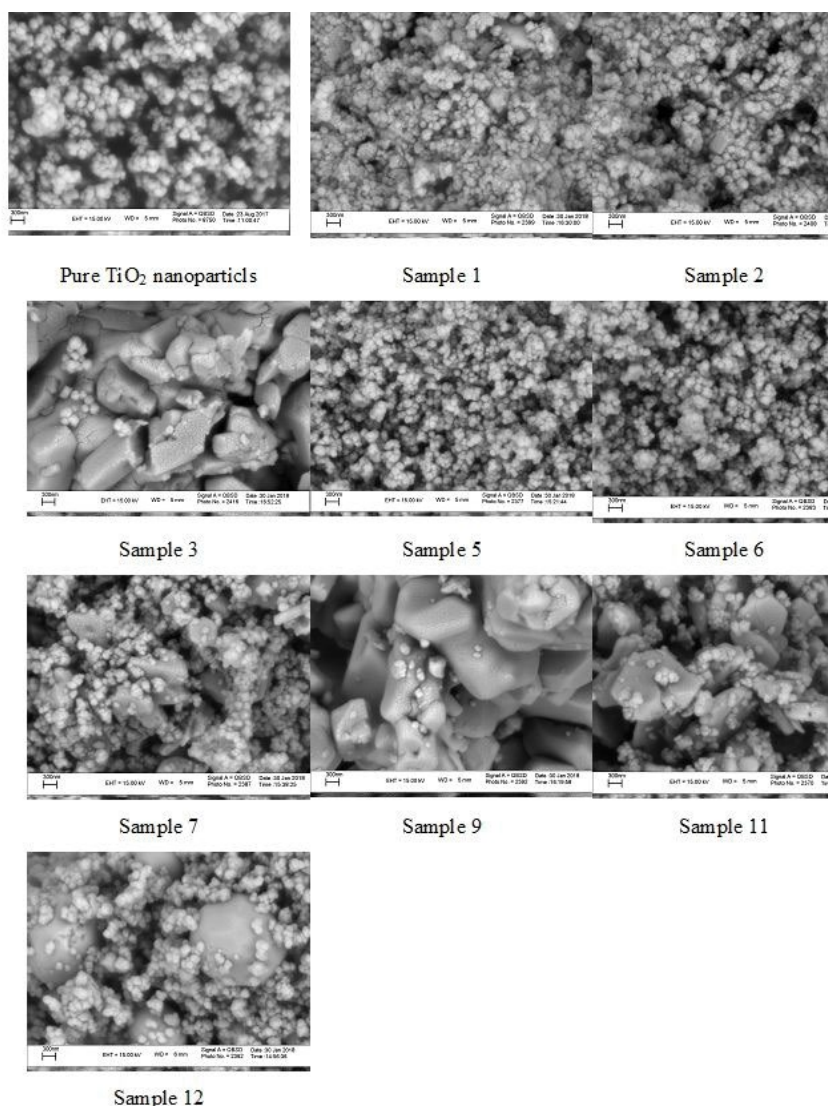


Fig. 3. SEM images of pure and co-doped TiO_2 powders.

the larger particles. In previous studies on iron, copper, and silver doped TiO_2 , only the spherical shaped and uniform sized (such as pure TiO_2 in the present study) nanoparticles were formed [5,6]. Therefore, it seems that the simultaneous presence of two different metal salts with higher concentration have a reduction effect on the melting point of the mixture, which results in the formation of larger particles.

3.2. Photocatalytic activity

The photocatalytic activity of pure and co-doped TiO_2 nanoparticles under visible light irradiation is illustrated in Fig. 4. In the absence of nanoparticles, no remarkable changes were observed in the concentration of the MO solution. Therefore, the MO decomposition only depends on the photo-excitation of nanoparticles. The results of Fig. 4 are summarized in Table 2. According to Fig. 4, the pure TiO_2 nanoparticles have the lowest dye removal rate of about 43% that only 7% of it is due to photocatalytic activity,

and the rest is due to dye absorption. As mentioned earlier, pure TiO_2 nanoparticles only have photocatalytic activity under UV light irradiation [18]. Since the visible light was used in this study to stimulate the photocatalytic activity, the pure TiO_2 nanoparticles exhibit very low photocatalytic activity. According to Fig. 4, most of the adsorption of MB by nanoparticles is done by sample 6, which has no silver content in its structure, and the minimum photocatalytic activity belongs to this sample. According to the SEM images, this sample is composed of small particles; therefore, it has a high surface area for adsorption. However, the band gap of this sample is 3.0 eV. Thus, it exhibits low photocatalytic activity.

The maximum dye removal activity due to photocatalytic activity and surface adsorption, which is about 94%, belongs to samples 1, 2, 5, and 7. According to the DRS and SEM results, sample 1 has the lowest band gap energy, and it is composed of spherical shaped with relatively the same small size particles; therefore, it shows high optical activity.

Table 3
Band gap of pure and co-doped TiO₂ powders

Sample	Band gap (eV)
0	3.2
1	2.82
2	2.91
3	2.85
5	2.98
6	3.00
7	3.00
9	2.88
11	2.92
12	2.99

On the other hand, the lowest amount of dye absorption belongs to this sample. However, in the case of samples 2, 5, and 7 the photocatalytic activity was lower than sample 1, but higher dye absorption has taken place.

Briefly, the increase in photocatalytic activity of optimum codoped TiO₂ nanoparticles is related to the enhancement of light (both UV and visible light) absorption, which enhances light energy for photocatalysis. Furthermore, smaller band gap leads to the easier formation of electron/hole pairs. Finally, smaller particle size provides a higher surface area for photocatalytic activity. Thus, all of these

parameters enhanced the photocatalytic performance of TiO₂.

Previous work on the photocatalytic activity of iron, silver, and copper doped TiO₂ nanoparticles synthesized by molten salt method yielded 60%, 78%, and 70% methyl orange dye removal efficiencies, respectively. The yield obtained in the present work is about 94%; therefore, it seems that co-doping and the presence of two dopants have a synergistic effect on the photocatalytic property. This result is consistent with Wang and Yamauchi [9] and Sharma et al. [10].

3.3. Response of solar photocatalytic degradation experiments and modeling

The experimental results obtained in the photocatalytic degradation runs are presented in Table 2 and were fitted with the suggested quadratic model by the Design Expert, which gave the following regression equations for degradation:

$$\begin{aligned} \text{Catalytic activity} = & +53.75370 + 54.20072 \times \text{Silver content} + \\ & 115.36027 \times \text{Zinc content} + 116.83677 \times \text{Silver content} \times \\ & \text{Zinc content} - 58.84524 \times \text{Silver content}^2 - 280.40908 \times \\ & \text{Zinc content}^2 \end{aligned} \quad (2)$$

The ANOVA results are summarized in Table 4. The ANOVA was used to check the significance and adequacy of the model. The degree of significance and accuracy of

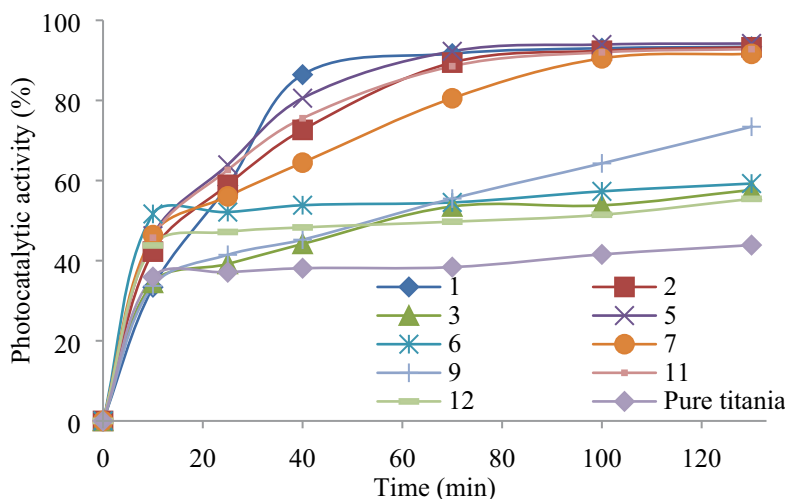


Fig. 4. Photocatalytic activity of the pure and co-doped TiO₂ powders.

Table 4
ANOVA analysis results for the photocatalytic degradation

Source	Sum of squares	Degree of freedom	Mean square	F-value	p-value
Model	2,551.738	5	510.3477	10.97373	0.0033
Silver content	39.80293	1	39.80293	0.855861	0.3857
Zinc content	739.0028	1	739.0028	15.89038	0.0053

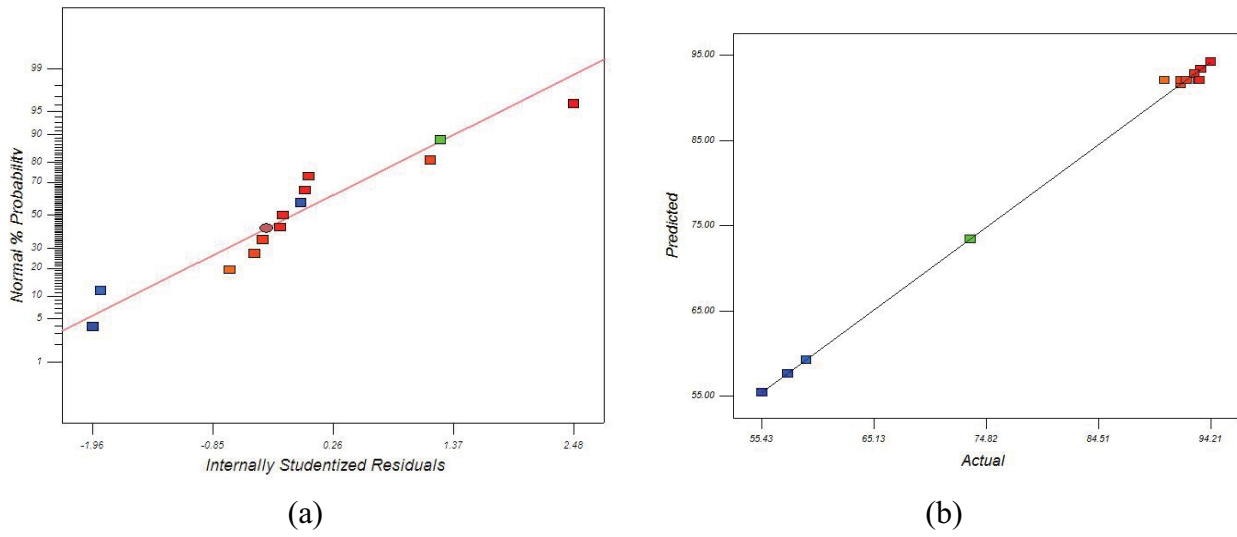


Fig. 5. (a) Normal probability plot of the experimental results of degradation efficiency and (b) plot of the predicted vs. the actual degradation efficiency.

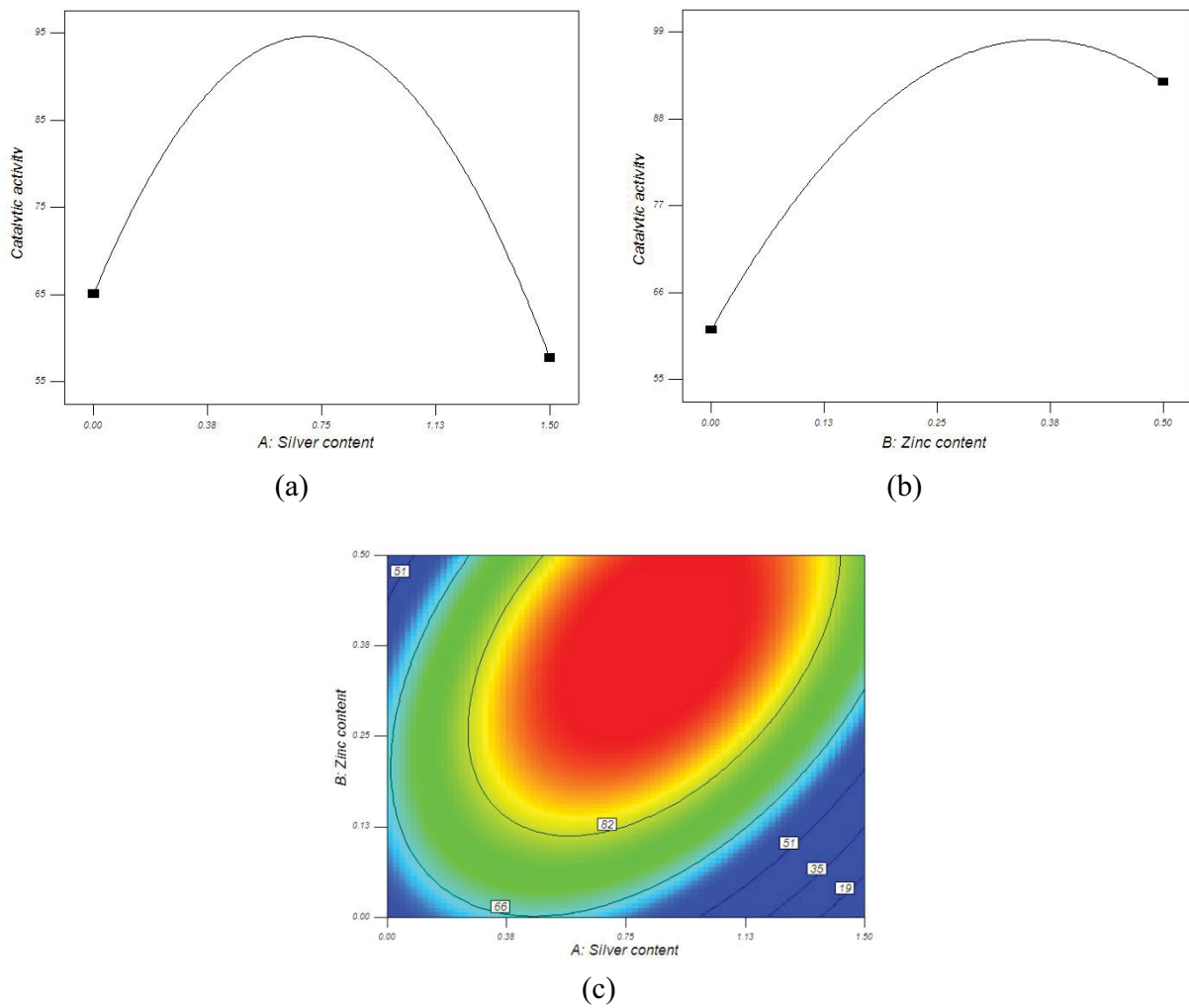


Fig. 6. Response surface plot of the degradation efficiency as the function of (a) silver content, (b) zinc content, and (c) silver and zinc content.

the proposed regression model were evaluated using the p -value, F -value, R^2 , and adjusted R^2 . The model is significant, with a 0.89% confidence interval since the p -value was 0.0033, which is less than 0.05. The analysis revealed that both factors are significant. The R^2 , and R^2 adjusted values, which were 0.8869, and 0.8060, respectively, show that a sufficient model was created. The adequacy precision was 7.931, which is larger than 4, indicates that the model is adequate.

Fig. 5 is a plot of the normal probability of the residuals. Accordingly, most of the obtained data points were consistently distributed on a straight trend line, which indicates the proper adequacy of the regression model utilized for degradation. Fig. 5b shows that the actual values were in good agreement with the predicted values, which indicated the adequacy and significance of the model. The plot should have random distribution (constant range of residuals across the graph).

The response surface plots provide the type of interaction between variables used to optimize the efficiency of photocatalytic activity. The effect of Zn and silver contents is shown in Fig. 6. The degree of degradation increased with increasing zinc content up to 38% and then decreased. On the other hand, the degree of degradation increased with increasing silver content up to 75% and then decreased. The simultaneous effects of Zn and silver content are shown in Fig. 6c. Degradation increased with increasing zinc and silver content, up to 38% and 75%, respectively. After exceeding this value, the degradation rate decreased.

According to previous studies, the presence of metal ion dopant enhances the photocatalytic activity because the catalyst activity modification is the effect of changes resulted from interface changes transfer, light absorption capacity of TiO_2 , and catalyst adsorption capacity of pollutant molecules [19]. On the other hand, doping with metals could introduce many oxygen vacancies in the crystal lattice and on the surface of TiO_2 , which favors the water concentration, the formation of surface hydroxyl groups, and the promotion of the photocatalytic activity [20]. However, when much dopant is doped, they can consume photo-induced electron and create holes. This can lead to a reduction of the photocatalytic activity. Therefore, there is an optimum dopant content in which the codoped TiO_2 separate the photo-induced electron-hole pair effectively and provide the best photocatalytic performance.

4. Conclusion

In the present work, Zn and Ag co-doped TiO_2 tri-metallic nanoparticles are synthesized by the molten salt method, which is applied as an effective nanophotocatalyst for the removal of the methyl orange from the aqueous media. Results show changing of the synthesis techniques trend in the wastewater treatment from the more achievement of a product with the desired properties to methods that are highly effective, economical, and environmentally friendly. In the pure and single metal doping TiO_2 nanoparticles, the only formed phase was the anatase. The silver, anatase, and rutile phase could be observed in the prepared nanoparticles. The pure titanium sample has a band gap of 3.2. According to Table 3, all samples have

a band gap below this value. The accumulated spherical particles with relatively the same size are seen in the pure samples. The SEM images show that co-doping results in the formation of larger particles. The experimental results showed that the prepared nanoparticles have a high photo-degradation tendency to remove methyl orange from the aqueous solution under visible light irradiation. The highest photocatalytic activity of 94.2% belongs to samples containing 0.38% silver and 0.13% zinc.

References

- [1] M. Ghorbanpour, M. Yousofi, S. Lotfiman, Photocatalytic decolorization of methyl orange by silica-supported TiO_2 composites, *J. Ultrafine Grained Nanostruct. Mater.*, 50 (2017) 43–50.
- [2] U.G. Akpan, B.H. Hameed, Parameters affecting the photocatalytic degradation of dyes using TiO_2 -based photocatalysts: a review, *J. Hazard. Mater.*, 170 (2009) 520–529.
- [3] R. Dagher, P. Drogui, D. Robert, Modified TiO_2 for environmental photocatalytic applications: a review, *Ind. Eng. Chem. Res.*, 52 (2013) 3581–3599.
- [4] N.N. Binitha, Z. Yaakob, M.R. Reshmi, S. Sugunan, V.K. Ambili, A.A. Zetty, Preparation and characterization of nano silver-doped mesoporous titania photocatalysts for dye degradation, *Catal. Today*, 147 (2009) S76–S80.
- [5] M. Madadi, M. Ghorbanpour, A. Feizi, Antibacterial and photocatalytic activity of anatase phase Ag-doped TiO_2 nanoparticles, *Micro Nano Lett.*, 13 (2018) 1590–1593.
- [6] M. Ghorbanpour, A. Feizi, Iron-doped TiO_2 catalysts with photocatalytic activity, *J. Water Environ. Nanotechnol.*, 4 (2019) 60–66.
- [7] M. Madadi, M. Ghorbanpour, A. Feizi, Preparation and characterization of solar light-induced rutile Cu-doped TiO_2 photocatalyst by solid-state molten salt method, *Desal. Water Treat.*, 145 (2019) 257–261.
- [8] A. Eini, M. Ghorbanpour, Evaluation the antibacterial effect of Zn-doped TiO_2 nanoparticles immobilized on the bentonite, *Nanomegnyas*, 6(2019) 21–29.
- [9] L. Wang, Y. Yamauchi, Strategic synthesis of tri-metallic Au@Pd@Pt core-shell nanoparticles from poly (vinylpyrrolidone)-based aqueous solution toward highly active electrocatalysts, *Chem. Mater.*, 23 (2011) 2457–2465.
- [10] G. Sharma, V.K. Gupta, S. Agarwal, S. Bhogal, M. Naushad, A. Kumar, F.J. Stadler, Fabrication and characterization of tri-metallic nano-photocatalyst for remediation of ampicillin antibiotic, *J. Mol. Liq.*, 260 (2018) 342–350.
- [11] Y. Cong, J. Zhang, F. Chen, M. Anpo, D. He, Preparation, photocatalytic activity, and mechanism of nano- TiO_2 co-doped with nitrogen and iron (III), *J. Phys. Chem. C*, 111 (2007) 10618–10623.
- [12] J. Tian, Z. Zhao, A. Kumar, R.I. Boughton, H. Liu, Recent progress in design, synthesis, and applications of one-dimensional TiO_2 nanostructured surface heterostructures: a review, *Chem. Soc. Rev.*, 43 (2014) 6920–6937.
- [13] M. Malekshahi Byranvand, A. Nemati Kharat, L. Fathollahi, Z. Malekshahi Beiranvand, A review on synthesis of nano- TiO_2 via different methods, *J. Nanostruct.*, 3 (2013) 1–9.
- [14] B. Roy, P.A. Fuierer, S. Aich, Synthesis of TiO_2 scaffold by a 2 step bi-layer process using a molten salt synthesis technique, *Powder Technol.*, 208 (2011) 657–662.
- [15] B. Roy, S.P. Ahrenkiel, P.A. Fuierer, Controlling the size and morphology of TiO_2 powder by molten and solid salt synthesis, *J. Am. Ceram. Soc.*, 91 (2008) 2455–2463.
- [16] M. Ghorbanpour, S. Lotfiman, Solid-state immobilisation of titanium dioxide nanoparticles onto nanoclay, *Micro Nano Lett.*, 11 (2016) 684–687.
- [17] A. Mohammed, A. Kadhum, M. Ba-Abbad, A. Al-Amiery, Optimization of solar photocatalytic degradation of chloroxylenol using TiO_2 , $\text{Er}^{3+}/\text{TiO}_2$, and $\text{Ni}^{2+}/\text{TiO}_2$ via the Taguchi orthogonal array technique, *Catalysts*, 6 (2016) 163.

- [18] A.A. Ashkarran, S.M. Aghigh, N.J. Farahani, Visible light photo-and bioactivity of Ag/TiO₂ nanocomposite with various silver contents, *Curr. Appl. Phys.*, 11 (2011) 1048–1055.
- [19] W.C. Hung, S.H. Fu, J.J. Tseng, H. Chu, T.H. Ko, Study on photocatalytic degradation of gaseous dichloromethane using pure and iron ion-doped TiO₂ prepared by the sol-gel method, *Chemosphere*, 66 (2007) 2142–2151.
- [20] M. Crişan, M. Răileanu, N. Drăgan, D. Crişan, A. Ianculescu, I. Niţoi, P. Oancea, S. Şomăcescu, N. Stănică, B. Vasile, C. Stan, Sol-gel iron-doped TiO₂ nanopowders with photocatalytic activity, *Appl. Catal., A*, 504 (2015) 130–142.